



Bernstein–Greene–Kruskal Ion Modes in Dusty Space Plasmas Application in Saturn’s Magnetosphere

Harikrishnan Arayindakshan^{1,2} , Amar Kakad¹ , Bharati Kakad¹ , and Ioannis Kourakis^{2,3} 

¹ Indian Institute of Geomagnetism, New Panvel, Navi Mumbai, 410218, India

² Department of Mathematics, College of Arts and Sciences, Khalifa University, Abu Dhabi, UAE

³ Space and Planetary Science Center, Khalifa University, Abu Dhabi, UAE

Received 2022 May 10; revised 2022 August 2; accepted 2022 August 2; published 2022 September 6

Abstract

Frequent observations of ion beams moving out from Saturn’s plasma environment hints at the generation of ion Bernstein–Greene–Kruskal (BGK) modes. As the plasma environments of Saturn and its moon Enceladus are characterized by the ubiquitous presence of massive negatively charged dust particles, the existing BGK theory for electron-ion plasma models cannot address this scenario. This manuscript develops a theoretical model for studying ion BGK modes in dusty plasmas. The analysis reveals that the presence of dust in the plasma enhances the stability of BGK modes. As the dust density increases, the effect of other parameters on stability, such as the electron temperature, becomes negligible. The model is developed by assuming that electrons and ions follow a kappa distribution, featuring a long tail trend in the superthermal component, in agreement with observations. Different scenarios with either electrons or ions obeying a Maxwell or kappa distribution function have been considered. A thorough analysis of the trapped ion distribution function considering various combinations indicates that a plasma where electrons are in thermal equilibrium and ions follow kappa distribution is the least favorable system for the generation of BGK modes.

Unified Astronomy Thesaurus concepts: [Saturn \(1426\)](#)

1. Introduction

Coherent bipolar electric field structures are ubiquitously observed in space and other astrophysical environments (Matsumoto et al. 1994; Franz et al. 1998; McFadden et al. 2003; Kakad et al. 2016; Wang et al. 2020; Singh et al. 2021; Kakad et al. 2022; Singh et al. 2022). In the kinetic framework, these structures are effectively modeled as Bernstein–Greene–Kruskal (BGK) modes (Bernstein et al. 1957). As there is an electrostatic monopolar potential associated with these bipolar electric fields, depending on the polarity of the potential, either electrons or ions with suitable energy will become trapped inside the potential. So, physically, BGK modes represent an equilibrium between trapped particles passing particles and the background plasma parameters (Krasovsky et al. 2003). From a theoretical perspective, these structures have a low density at the center and a high density at the rim in phase space. Hence these structures are also called electron or ion holes depending on the charge of the trapped particle (Eliasson & Shukla 2006b). Omura et al. (1996) established that streaming instabilities are the reason behind the generation of BGK modes. Interestingly, a series of experimental investigations of ion holes by Pécseli et al. (1981, 1984) showed that ion holes may be excited by an ion two-stream instability in laboratory plasma. Subsequent laboratory studies focused on three-dimensional ion BGK modes triggered in the laboratory, studying their generation and dynamic evolution (Pécseli 1987; Franck et al. 2001) Recently, Wang et al. (2020) showed that ion streaming instabilities favor the generation of ion holes using the observations from the Earth’s bow shock region.

As regards the modeling of BGK modes, there are two main theoretical approaches: the integral solution or BGK methodology and the differential (or Schamel) technique. In the former method (BGK), one assumes that the initial particle distribution function and the electrostatic potential profiles are known, so these are substituted into the Poisson equation and the integral equation is solved to obtain the trapped particle distribution function (Bernstein et al. 1957; Arayindakshan et al. 2018a, 2018b, and the references therein). In Schamel’s approach, the form of the trapped particle distribution function and of the passing (i.e., free, nontrapped) particle distribution function is assumed and substituted in Poisson’s equation, leading to a differential equation that is then solved to obtain the form of the potential (Schamel 1986; Luque & Schamel 2005, and the references therein). A distinguishing factor in the former (BGK) approach is that it involves a condition in the form of an inequality to be satisfied by the potential parameters (width and amplitude) in order for a BGK mode to be sustained. The BGK approach will be adopted in this work. The above models tacitly assume a collisionless electron-ion plasma. These assumptions are acceptable in the Earth’s magnetosphere. However, as we move farther from near-Earth plasma environments, the presence of charged dust in the plasma cannot be neglected. In the case of Saturn, there are observations of streaming ions by the Cassini spacecraft (Badman et al. 2012a, 2012b). We know that these streaming ion flows can lead to the generation of ion holes. Electrostatic solitary waves have been observed in Saturn’s magnetosphere (Williams et al. 2006) and in the dusty environment near its moon Enceladus (Pickett et al. 2015). Williams et al. (2006) reported observations of solitary structures in the vicinity of Saturn’s magnetosphere. They detected a series of bipolar pulses and speculated that these could be either electron holes or ion holes (Williams et al. 2006). Later on, Pickett et al. (2015) observed solitary wave pulses within 10 Rs (Rs is the

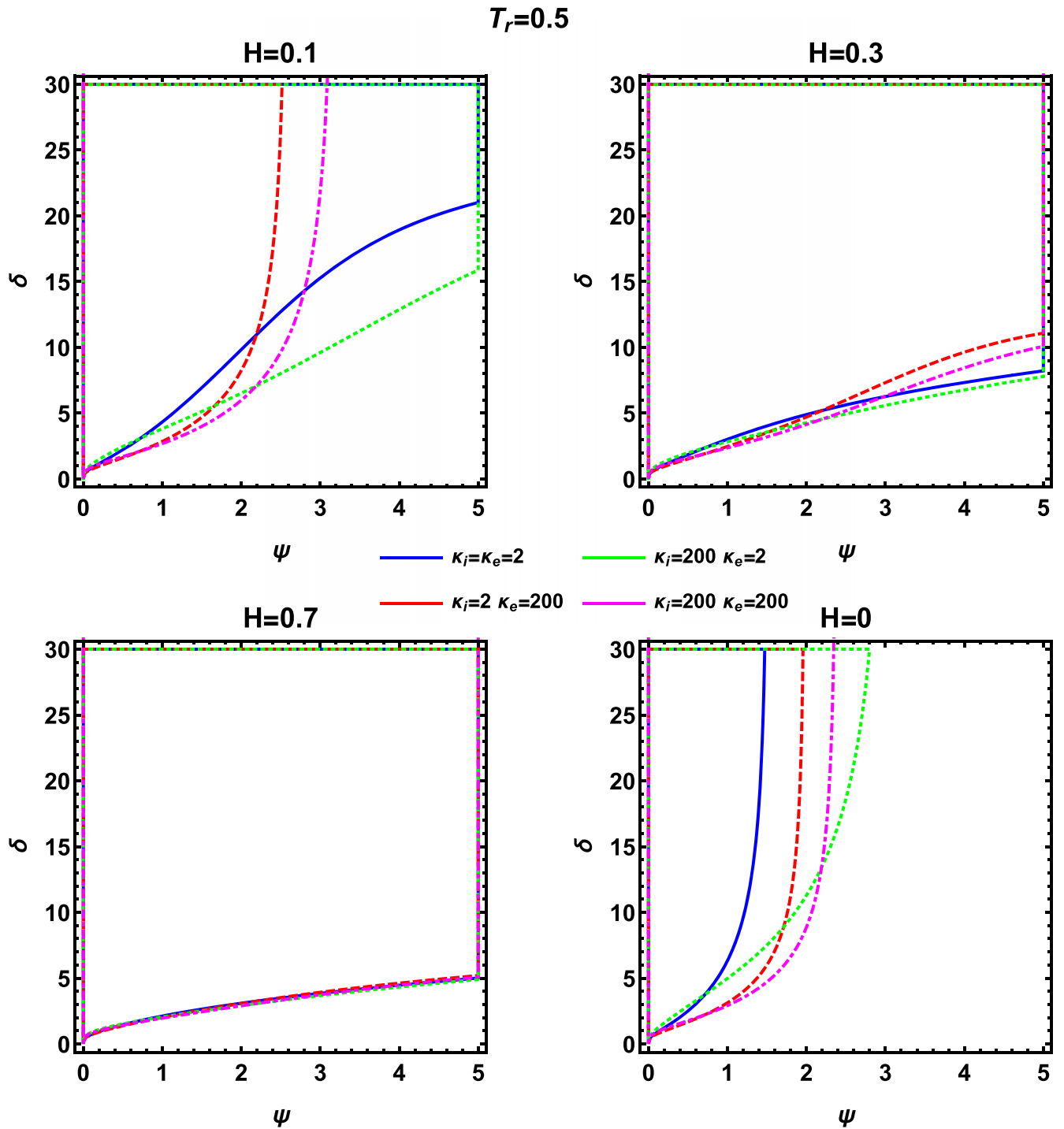


Figure 1. The width-amplitude relation for various Havnes parameters (H) is shown. Here κ_e and κ_i are the superthermal indices of electrons and ions, respectively. The blue line shows the case where both species are superthermal. The dotted green line denotes the case of thermal ions and superthermal electrons. The dashed red line indicates the case of superthermal ions and thermal electrons. The dot-dashed magenta line depicts the case of thermal electrons and ions. The area marked by the curves indicates the allowed region, and the area below the marked region indicates the restricted region. Here, the ion-to-electron temperature ratio (T_r) is 0.5.

Saturn radius) and near Enceladus. Near the Enceladus plume, they discussed how dust impacts affected the observed solitary waves. In fact, Pickett et al. (2015) pointed out that some of the bipolar electric field pulses associated with the solitary waves observed had an inverse polarity (i.e., a positive pulse first, followed by a negative pulse in a short time period) and suggested that this might be due to either an inverse direction of propagation or to a true inverse potential pulse polarity (sign). Moreover, Farrell et al. (2017) examined the conditions

that allow low-energy ions, such as those produced in the Enceladus plume, to be attracted and trapped within the sheath of negatively charged dust grains. Using particle-in-cell simulations, they showed that with dust in the system, the large electric field from the grain charge disrupts pickup and leads to ion trapping. Their simulation results also reveal that the bipolar pulses reported in the Enceladus plume by Williams et al. (2006) and Pickett et al. (2015) could most probably be ion holes. In the light of the above information, we may suggest

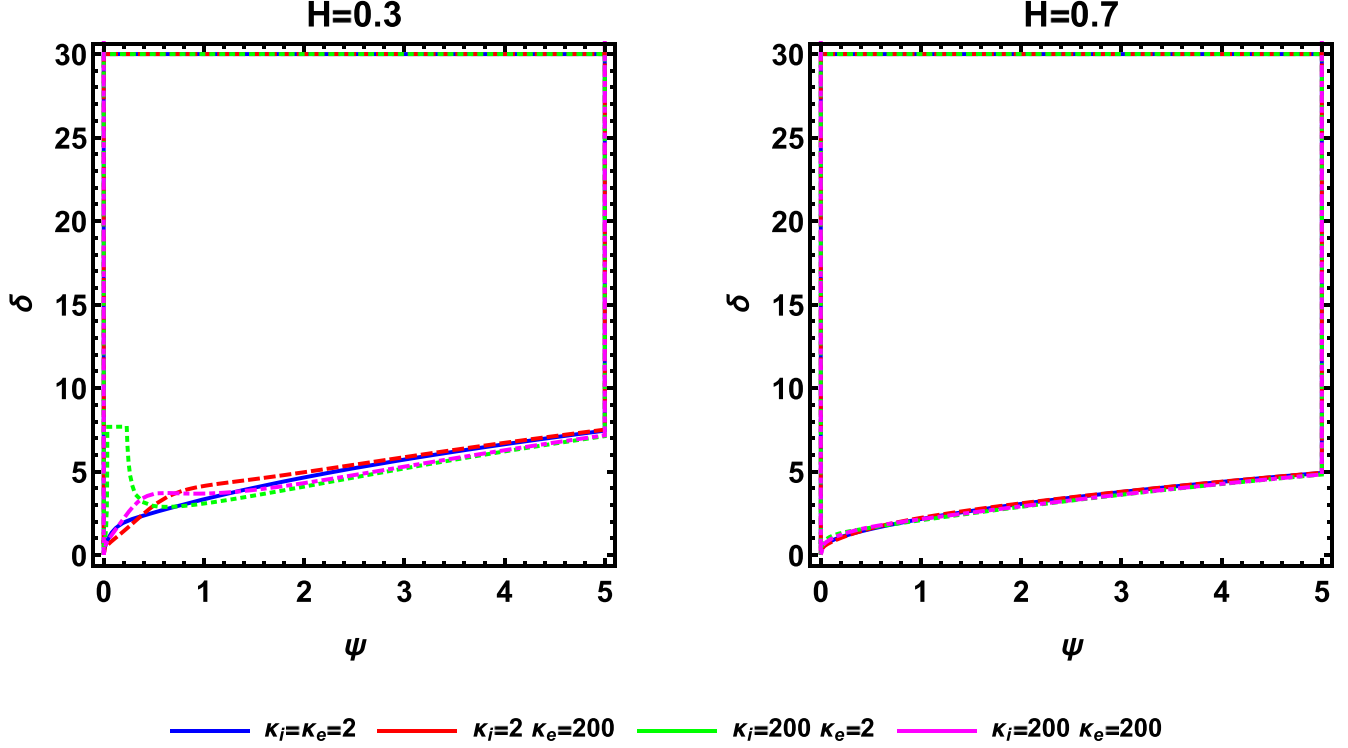
$T_r=3$ 

Figure 2. The width-amplitude relation for various Havnes parameters (H) is shown. Here κ_e and κ_i are the superthermal indices of electrons and ions, respectively. The blue line shows the case where both species are superthermal. The dashed red line indicates the case of superthermal ions and thermal electrons. The dotted green line denotes the case of thermal ions and superthermal electrons. The dot-dashed magenta line depicts the case of thermal electrons and ions. The area marked by the curves indicates the allowed region, and the area below the marked region indicates the restricted region. Here, the ion-to-electron temperature ratio (T_r) is 3.

that the formation of ion holes is highly likely in the dusty plasma of environments such as the one found in Saturn. Importantly, the instrument on board Cassini, the Radio Plasma Wave Science instrument, does not have the ability to determine the polarity of the electric fields associated with the ESWs observed with 100% certainty as it lacks the ability to perform interferometry (Williams et al. 2006).

Eliasson & Shukla (2006a) developed a theoretical model for the interaction of Langmuir envelope solitons with dust acoustic, dust ion acoustic, and ion hole-type excitations. They have included the effect of the dust on ion hole excitations and how it affects the relation between Langmuir wave envelopes and the electric potential. However, the role of dust in the generation of ion holes and how the dust affects the stability and characteristics of ion holes was not addressed in these studies. Because the Havnes parameter in Saturn's magnetosphere and its moon varies from 10^{-3} to as high a value as 0.7 (Yaroshenko et al. 2007; Yaroshenko & Lühr 2016), it is important to understand how dust affects the characteristics of ion holes. We recall that the Havnes parameter represents the ratio of the dust charge density to the ion charge density. The presence of dust in considerable density brings up a different nature to the plasma, and existing theories do not address ion-hole formation in these plasma environments (unless the dust component is explicitly taken into account, that is).

The aim of the present work is to develop a theoretical model that describes ion holes formed in dusty plasmas. The paper is organized as follows. In Section 2 we discuss the mathematical (kinetic) modeling aspects and establish a new framework for dust-ion BGK type excitations (holes). A parametric analysis is

carried out, and the results are presented and discussed in Section 3. Finally, our findings are summarized in Section 4.

2. Theoretical Modeling

We consider a one-dimensional collisionless electrostatic plasma system consisting of electrons, ions with charge state Z_i , and negatively charged dust with charge state Z_d (assumed constant). As the dust particles are extremely heavy, the density of the dust is assumed to be constant. Taking into account three charged species, the Poisson equation is given by

$$\nabla^2 \phi = -\frac{e}{\epsilon_0} (Z_i n_i - n_e - Z_d n_d) \quad (1)$$

.Here ϕ is the electrostatic wave potential, n_i , is the ion density, n_e is the electron density, and n_d is the dust density. For the sake of analytical tractability and ease of presentation, it is appropriate to consider rescaling the above equation. We use the plasma period—i.e., the inverse of the ion plasma frequency $\omega_{p,i}^{-1} = \left(\frac{n_{i,0} Z_i^2 e^2}{\epsilon_0 m_i} \right)^{-1/2}$ —to normalize the time variable; the velocity variable is normalized by $\left(\frac{2k_B T_i}{m_i} \right)^{1/2}$; the electrostatic potential is normalized by $\frac{k_B T_i}{Z_i e}$, and the space variable is normalized over the ion Debye length, $\left(\frac{k_B T_i \epsilon_0}{n_{i,0} Z_i^2 e^2} \right)^{1/2}$. The density variables n_i , n_e , and n_d are normalized by $Z_i n_{i,0}$.

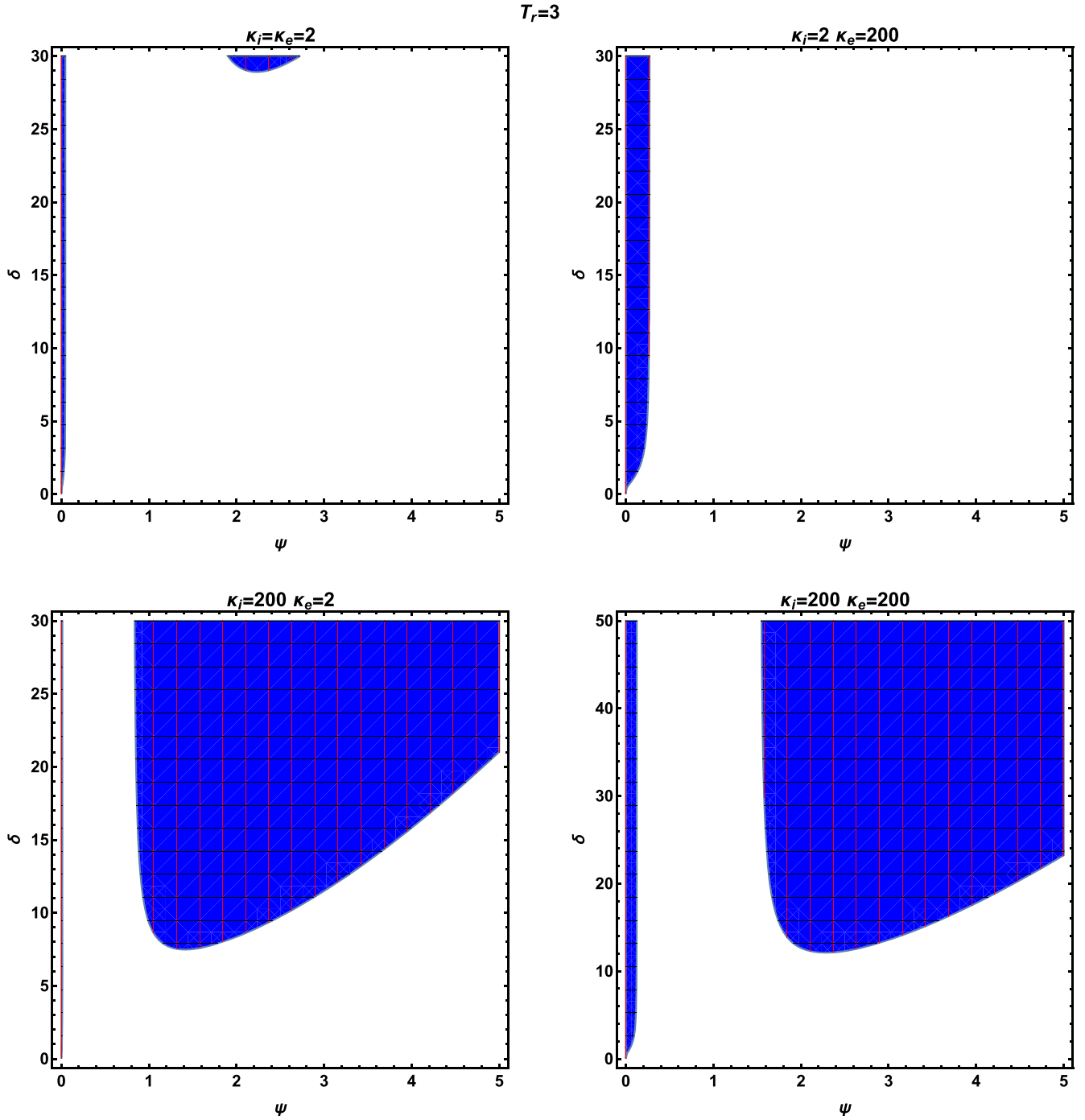


Figure 3. The width-amplitude plot is shown in the case where the Havnes parameter is kept at $H = 0$, i.e., in the absence of dust (electron-ion plasma), as depicted in the ion-hole theory developed by Aravindakshan et al. (2020) while taking $T_r = 3$, considering various kappa index values. Here κ_e and κ_i denote the superthermal indices of electrons and ions, respectively. The blue region is the allowed region, and the other region is the restricted region. If the potential has the width and amplitude of the blue region, it can support a physically plausible ion hole. It does not support the existence of ion holes if this condition is not met.

Poisson's equation thus takes the dimensionless form

$$\frac{d^2\phi}{dx^2} = (1 - H)n_e - n_i + H. \quad (2)$$

Here, $H = \frac{Z_d n_{d,0}}{Z_i n_{i,0}}$ is the Havnes parameter (Shukla & Mamun 2015).

It is by now established that space and astrophysical plasmas are not in thermal equilibrium, but present a strong energetic particle presence in the superthermal region of the velocity

distribution. Such plasmas can be effectively modeled by kappa distribution function given by Equation (4). Hence, we assume the electrons and ions to follow a kappa distribution. Taking the first moment of the electron distribution function, we obtain the electron density, given by

$$n_e = \left(1 - \frac{T_r \phi}{\kappa_e - \frac{3}{2}}\right)^{\frac{1}{2} - \kappa_e}. \quad (3)$$

$T_r=3$

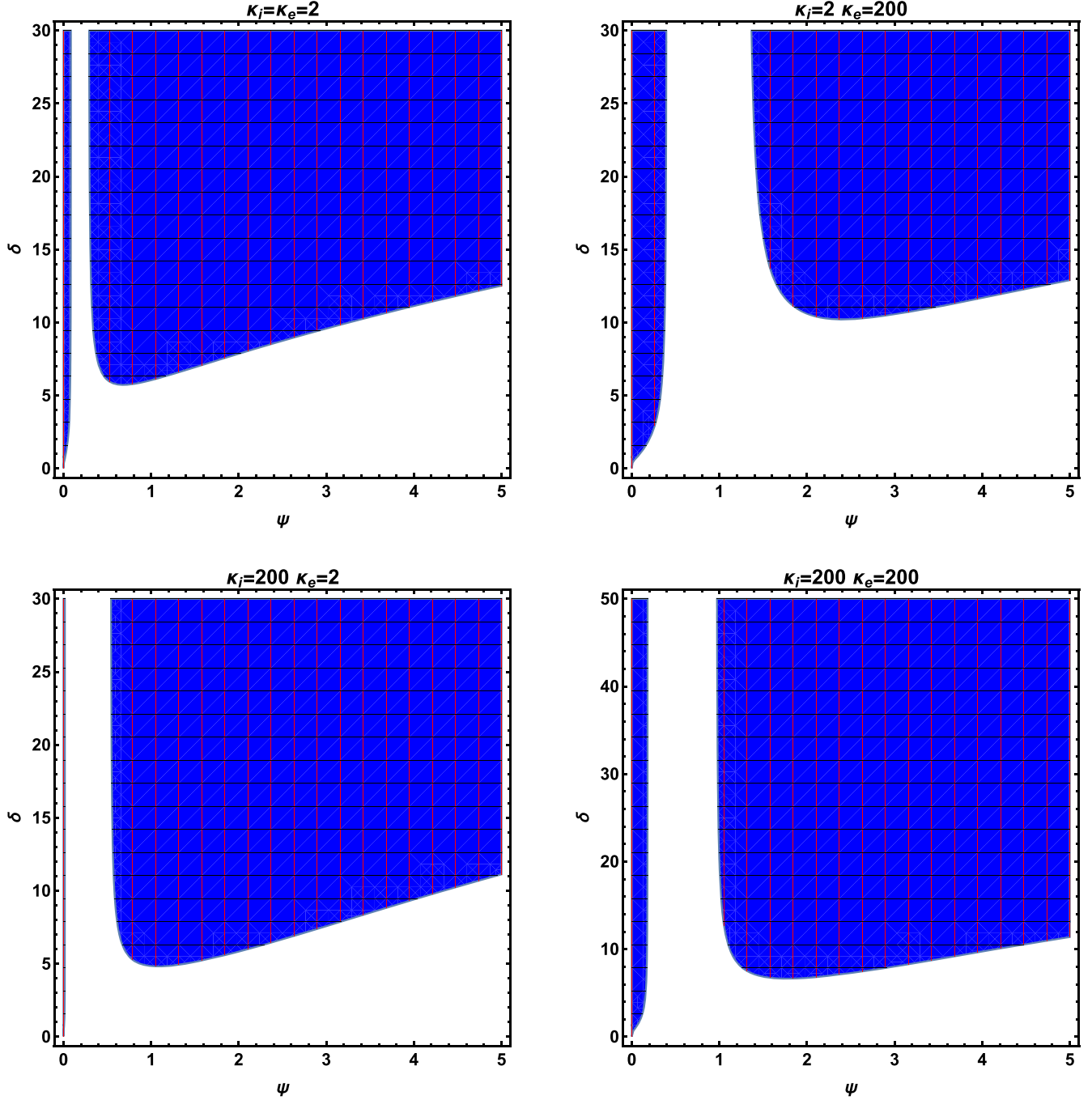


Figure 4. The width-amplitude plot is shown in the case where the Havnes parameter is kept at $H = 0.1$, while $T_r = 3$, considering various kappa index values. Here κ_e and κ_i denote the superthermal indices of electrons and ions, respectively. The blue region is the allowed region, and the other region is the restricted region. If the potential has the width and amplitude of the blue region, it can support a physically plausible ion hole. It does not support the existence of ion holes if this condition is not met.

Here, we have defined $T_r = T_i/T_e$, while κ_e denotes the superthermal index of adiabatic electron. As mentioned above, the ions follow a superthermal distribution (Livadiotis & McComas 2013; Hellberg et al. 2009; Hapgood et al. 2011) of the form

$$f_i(v) = \frac{\Gamma(\kappa_i + 1)}{\sqrt{\pi} \kappa_i \Gamma(\kappa_i - 1/2) \sqrt{\kappa_i - 3/2}} \left(\frac{v^2}{\kappa_i - 3/2} + 1 \right)^{-\kappa_i}, \quad (4)$$

where Γ denotes the Gamma function. Note that the ion and electron distribution functions are characterized by different values of the respective spectral index, κ_e , κ_i , in agreement with existing observations and as actually intuitively expected (given the large mass disparity between these two particles and thus the difference in the two populations' response to thermalization mechanisms). Note that κ_e and κ_i always assume values greater than $3/2$ to preserve the reality of all state variables.

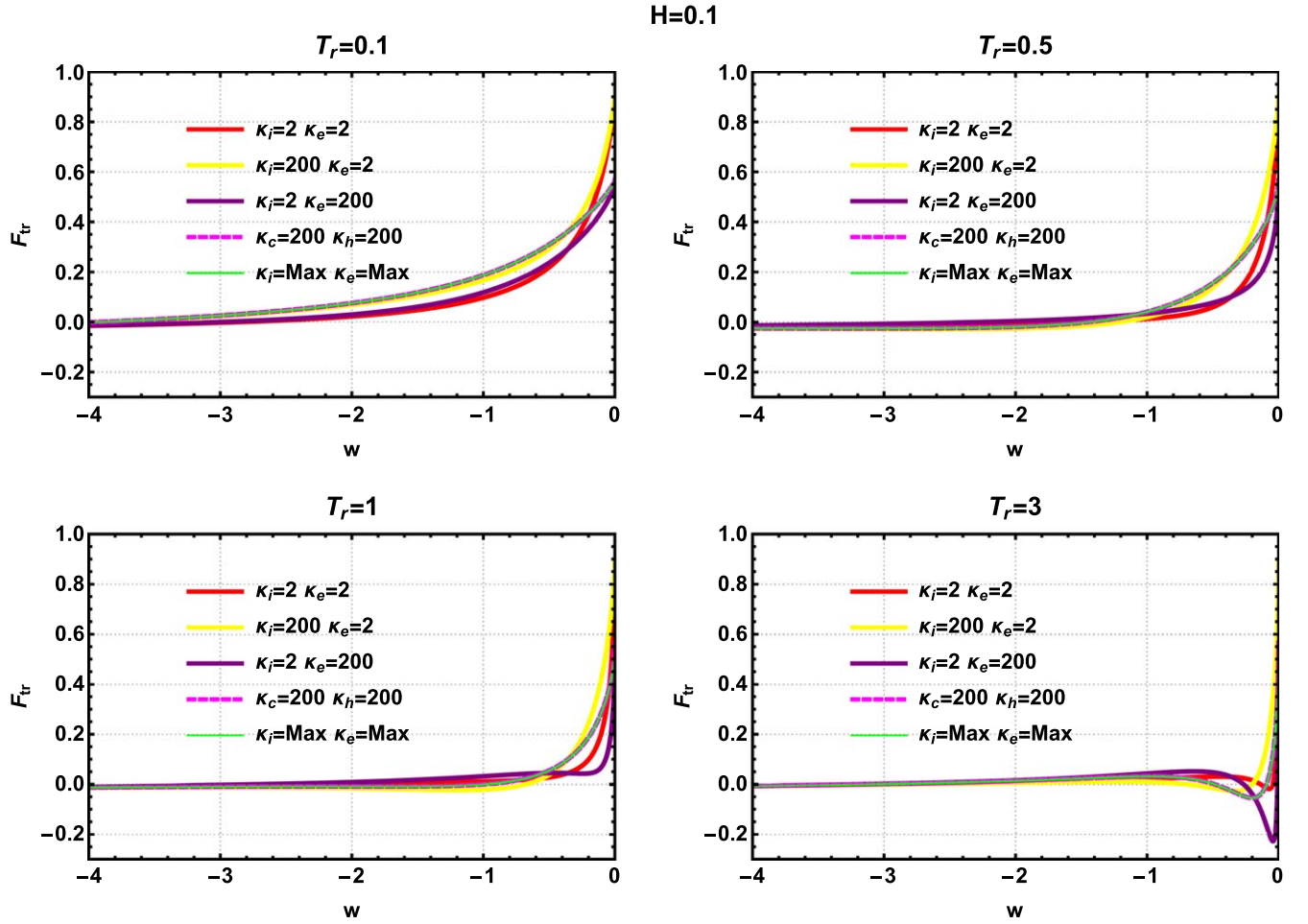


Figure 5. The variation in the trapped ion distribution function is plotted against the total energy w for various kappa index combinations. Here, the Havnes parameter H is set to 0.1, while $\psi = 2$ and $\delta = 20$. The different subpanels show the variation of the trapped ion distribution function for various values of the temperature ratio. Here red, yellow, violet, magenta, and green lines shows the cases of superthermal electrons and ions, thermal ions and superthermal electrons, superthermal ions and thermal electrons, thermal electrons and ions, and electrons and ions that follow a Maxwellian distribution other than the approximated values, respectively.

Following the original BGK kinetic-theoretical scheme (Bernstein et al. 1957), we transform the above equations to the energy frame, defined as

$$w = \frac{1}{2}(v^2 + \phi). \quad (5)$$

In the energy frame, the ion distribution transforms into

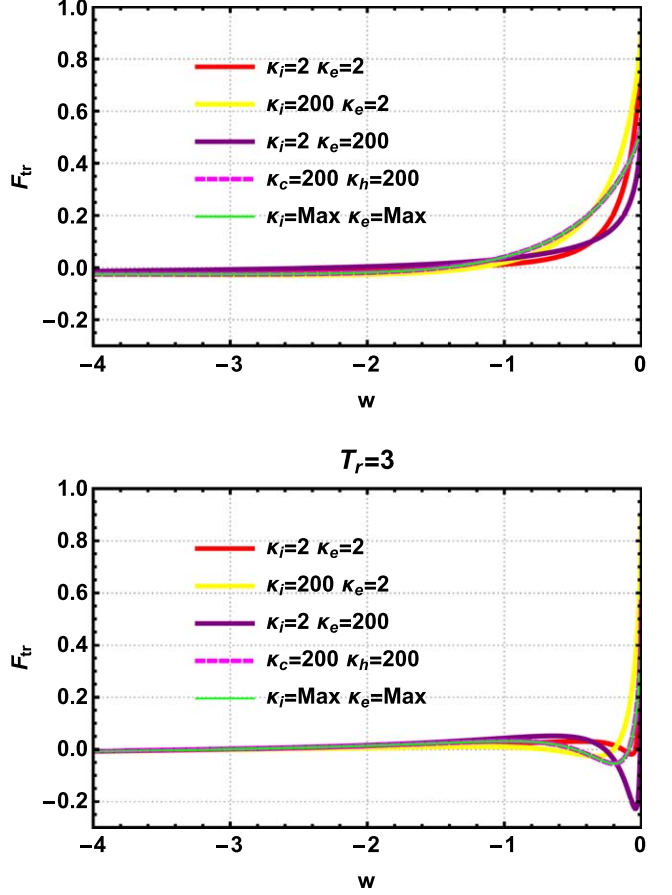
$$f_i(w) = \frac{\Gamma(\kappa_i)}{\sqrt{\pi} \sqrt{\kappa_i - 3/2} \Gamma(\kappa_i - 1/2)} \left(1 + \frac{2w}{\kappa_i - 3/2}\right)^{-\kappa_i}, \quad (6)$$

where

$$f(x, v)dv = f(w)dw/\sqrt{2w - \phi}. \quad (7)$$

Here, the total energy (w) is normalized with $mv_{th,i}^2$, i.e., $2k_B T_i$. As the ions encounter a negative potential well (a pulse), depending on their respective velocities, some of them will become trapped and some of them will pass through. Hence two types of population exist: a trapped population, and a passing population. We assume the passing populations to follow the initial distribution function - a kappa distribution function. In addition, we also assume the form of the potential in which

$H=0.1$



particles are trapped to be prescribed. Spacecraft observations show that wave potential structures of Gaussian form are common in space and astrophysical plasmas (Matsumoto et al. 1994; Williams et al. 2006). A negative wave potential well acts as a perturbation capable of trapping ions in it. We assume this potential well to have Gaussian form, given by

$$\phi(x) = -\psi \exp\left(-\frac{x^2}{2\delta^2}\right), \quad (8)$$

where ψ (>0) denotes the amplitude, and δ is the width of the perturbation, respectively. More precisely, δ is actually the distance where the potential decreases to 0.6065 times the maximum amplitude of ψ . The FWHM of the perturbation is actually given by $\Delta = 2.35\delta$. The net charge density can thus be expressed as

$$\frac{d^2\phi}{dx^2} = (1 - H)n_e - n_{i,p} - n_{i,tr} + H, \quad (9)$$

where $n_{i,p}$ is the passing ion density, and $n_{i,tr}$ is the trapped ion density. Particles with suitable velocities falling in the potential range $[-\sqrt{-\phi}, +\sqrt{-\phi}]$ will become trapped, and the rest will pass through. Thus, the range of integration for both passing

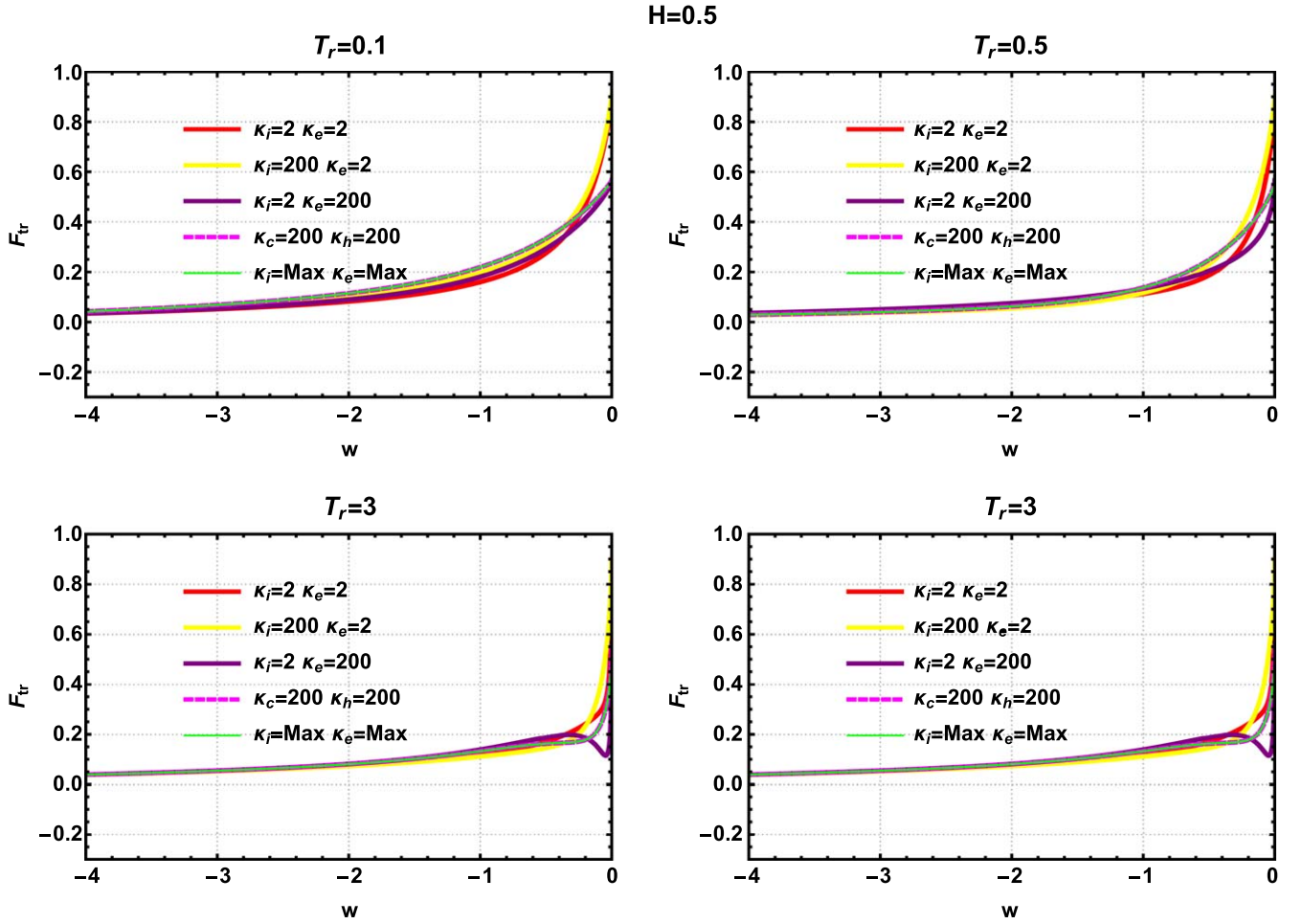


Figure 6. As in the previous figure, but with higher H (stronger dust concentration): the variation in the trapped ion distribution function is plotted against the total energy w for various kappa index combinations. Here, the Havnes parameter H is set to 0.5, while $\psi = 2$ and $\delta = 20$. The different subpanels shows the variation of the trapped ion distribution function for various values of the temperature ratio. Here red, yellow, violet, magenta, and green lines show the cases of superthermal electrons and ions, thermal ions and superthermal electrons, superthermal ions and thermal electrons, thermal electrons and ions, and electrons and ions that follow a Maxwellian distribution other than the approximated values, respectively.

and trapped ion distributions is given by

$$n_{i,p} = \int_{-\infty}^{-\sqrt{-\phi}} f_p(x, v) dv + \int_{+\sqrt{-\phi}}^{\infty} f_p(x, v) dv. \quad (10)$$

As the passing ions follow the kappa distribution, we obtain the passing ion density as

$$n_{i,p} = 1 - \frac{2A}{\sqrt{B}} \sqrt{-\phi} {}_2F_1[\kappa_i, 1/2, 3/2; \phi/B], \quad (11)$$

where ${}_2F_1$ is the hypergeometric function of the first kind. Now that we have obtained the passing ion density, we move on to the derivation of the trapped ion density. In terms of distribution function, the trapped ion density is given by

$$n_{i,tr} = \int_{-\sqrt{-\phi}}^{+\sqrt{-\phi}} f_{tr}(x, v) dv. \quad (12)$$

We may now derive the trapped ion density by rearranging Equation (9) as

$$n_{i,tr} = (1 - H)n_e - n_{i,p} - \frac{d^2\phi}{dx^2} + H. \quad (13)$$

Substituting from Equation (11) and differentiating the potential in Equation (8) twice, in Equation (13), we obtain the trapped electron density as

$$\begin{aligned} n_{i,tr} = (1 - H) & \left(1 - \frac{T_r \phi}{(\kappa_e - 3/2)} \right)^{0.5 - \kappa_e} \\ & + \frac{2\phi \log\left(-\frac{\phi}{\psi}\right)}{\delta^2} + \frac{\phi}{\delta^2} \\ & - 1 + \frac{2A}{\sqrt{B}} \sqrt{-\phi} {}_2F_1[\kappa_i, 1/2, 3/2; +\phi/B] + H. \end{aligned} \quad (14)$$

For convenience, we make a transformation $-\phi = |\phi| \rightarrow \rho$, (>0), and we obtain the trapped ion density as

$$\begin{aligned} n_{i,tr} = (1 - H) & \left(\frac{\rho T_r}{(\kappa_e - 3/2)} + 1 \right)^{0.5 - \kappa_e} - \frac{2\rho \log\left(\frac{\rho}{\psi}\right)}{\delta^2} \\ & - \frac{\rho}{\delta^2} - 1 + \frac{2A}{\sqrt{B}} \sqrt{\rho} {}_2F_1[\kappa_i, 1/2, 3/2; -\rho/B] + H. \end{aligned} \quad (15)$$

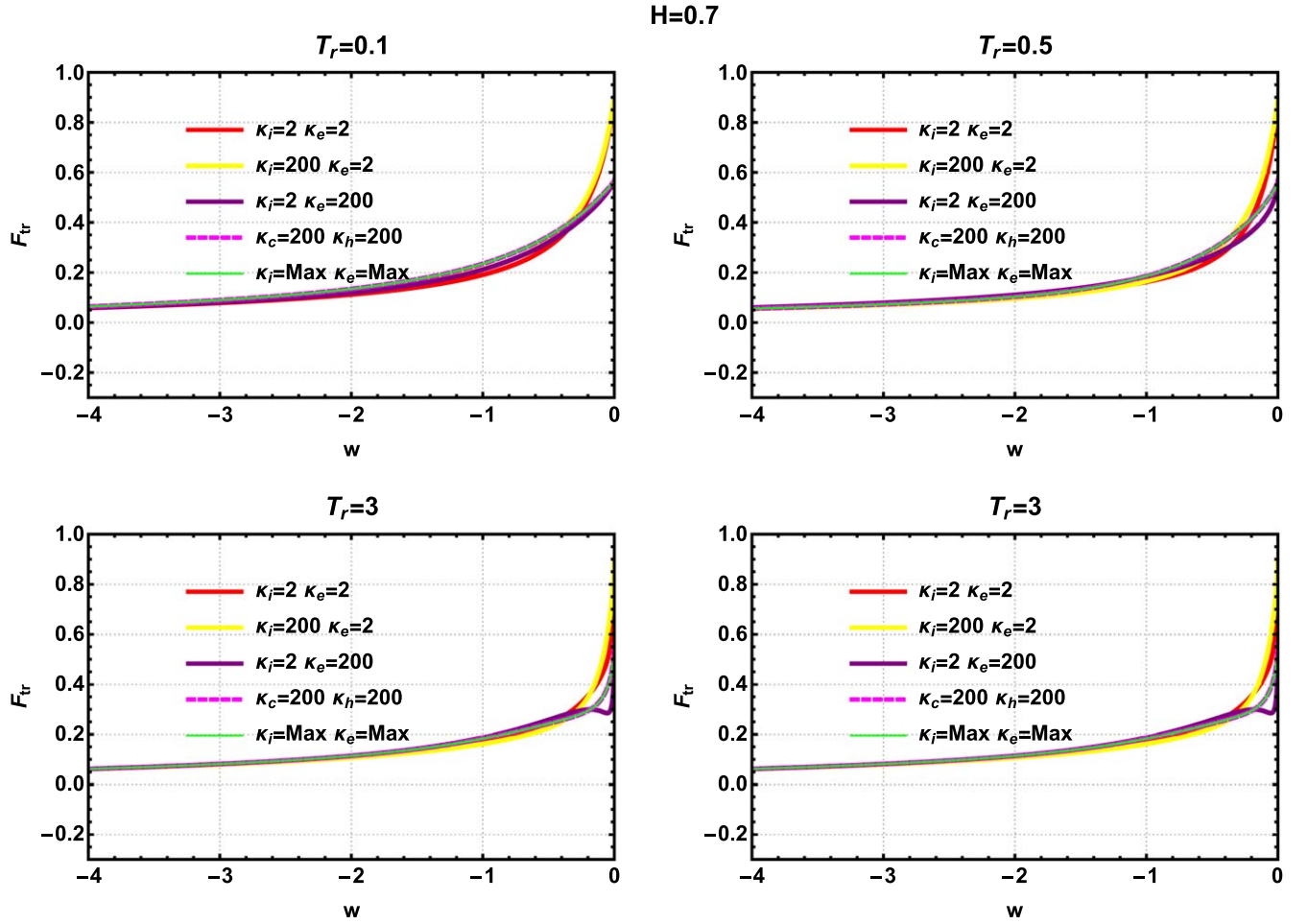


Figure 7. As in the latter two figures, but with an even higher H (stronger dust concentration): the variation in the trapped ion distribution function is plotted against the total energy w for various kappa index combinations. Here, the Havnes parameter H is set to 0.7, while $\psi = 2$ and $\delta = 20$. The different subpanels show the variation of the trapped ion distribution function for various values of the temperature ratio. Here red, yellow, violet, magenta, and green lines show the cases of superthermal electrons and ions, thermal ions and superthermal electrons, superthermal ions and thermal electrons, thermal electrons and ions, and electrons and ions that follow a Maxwellian distribution other than the approximated values, respectively.

The trapped ion density can be written as an integral of the trapped ion distribution function following Equation (12). Thus the trapped ion density can be represented as

$$\begin{aligned}
 2 \int_0^{+\sqrt{\rho}} f_{tr}(x, v) dv &= (1 - H) \left(\frac{\rho T_r}{\left(\kappa_e - \frac{3}{2}\right)} + 1 \right)^{0.5 - \kappa_e} \\
 &- \frac{2\rho \log\left(\frac{\rho}{\psi}\right)}{\delta^2} - \frac{\rho}{\delta^2} - 1 \\
 &+ \frac{2A}{\sqrt{B}} \sqrt{\rho} {}_2F_1\left[\kappa_i, 1/2, 3/2; -\rho/B\right] + H. \quad (16)
 \end{aligned}$$

In the w frame, the above equation can be represented as

$$2 \int_{-\rho/2}^0 \frac{f_{tr}(w)}{\sqrt{2w + \rho}} dw = g(\rho). \quad (17)$$

Here $g(\rho)$ is the right-hand side (RHS) of Equation (16).

To solve the above integral equation, we have adopted the method described in Aravindakshan et al. (2018a). The trapped

ion distribution function was thus found to be

$$\begin{aligned}
 f_{tr}(w) &= -(1 - H) \\
 &\times \frac{0.9(\kappa_e - 1/2) T_r \sqrt{-w} {}_2F_1\left(1, \kappa_e + 1/2; \frac{3}{2}; \frac{4T_r w}{2\kappa_e - 3}\right)}{\kappa_e - 3/2} \\
 &+ \frac{A {}_2F_1\left(\frac{1}{2}, \kappa_i; 1; \frac{2w}{B}\right)}{\sqrt{B}} - \frac{4\sqrt{2} \sqrt{-w} \left(\log\left(-\frac{8w}{\psi}\right) - 2\right)}{\pi \delta^2} \\
 &- \frac{6\sqrt{2} \sqrt{-w}}{\pi \delta^2}. \quad (18)
 \end{aligned}$$

The RHS of Equation (18) represents the trapped ion distribution function for the BGK modes formed in dusty plasmas. A close look at the distribution function reveals that the first term stems from the electron density part, and the Havnes parameter is attached to this term. The distribution function should be positive in order to represent a physically plausible scenario. It should be noted that the contribution of the electrons is regulated by the dust-related coefficient $1 - H$ and in fact disappears if $H = 1$ (total electron depletion, a scenario encountered, e.g., in cometary environments). It is

$$T_r=0.5$$

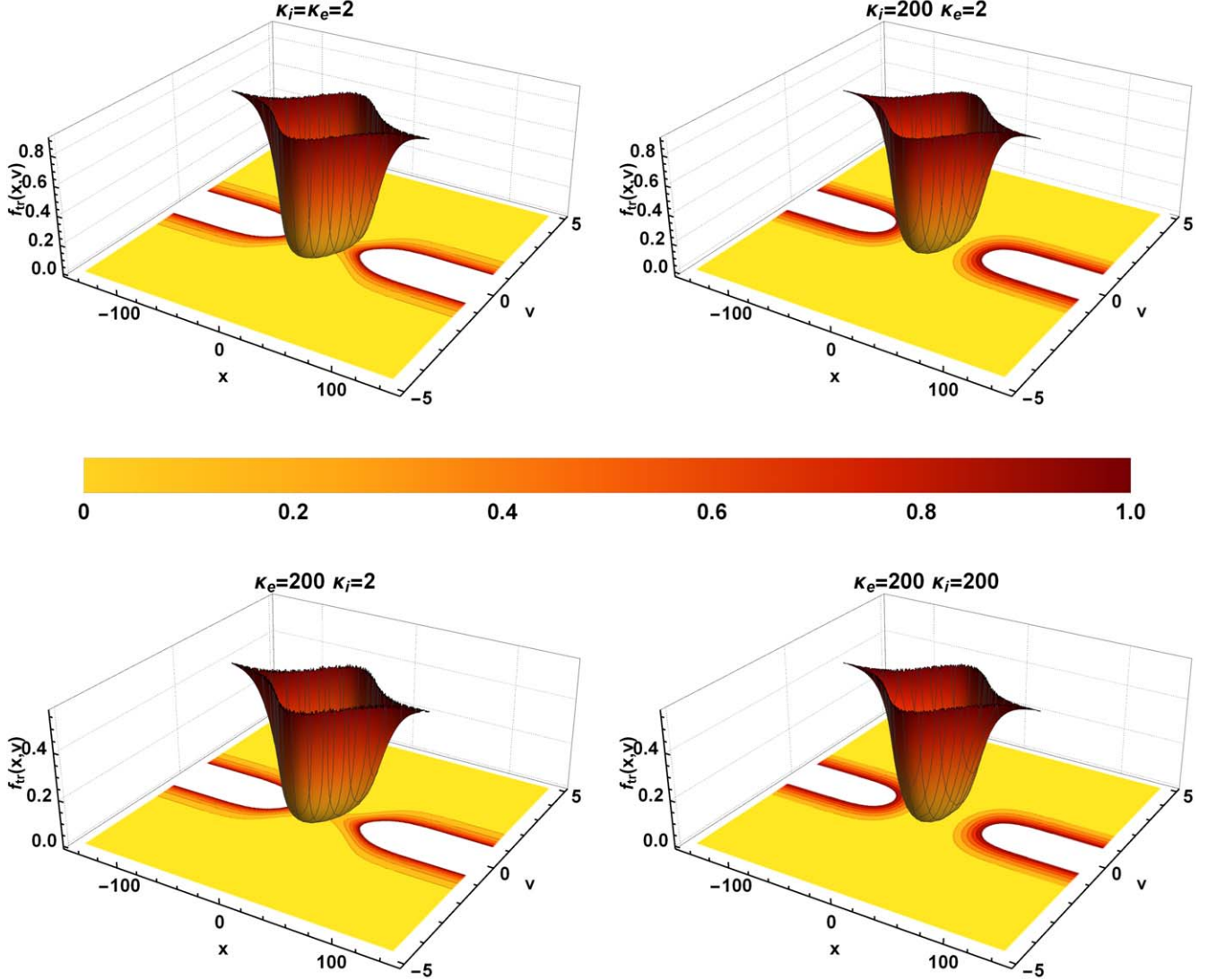


Figure 8. The structure of the trapped ion distribution function is depicted here. The Havnes parameter H is set to 0.1. Here $T_r = 0.5$, and the different panels show the trapped ion distribution function for various kappa indices. These combinations of kappa indices essentially constitute different space plasma scenarios. At the bottom, the contour plot of the passing distribution function is also given.

evident that the dust parameter H contributes toward maintaining the positive nature of the distribution function. The third and fourth terms in the above expression, stemming from the total charge density and the electron parameter, adversely affect the generation of an ion-hole equilibrium.

As mentioned above, this model can also be used to study BGK modes that formed in plasma configurations where either (or both) of the species is (are) in thermal equilibrium. The details of BGK modes (ion holes) in thermal (Maxwellian) dusty plasma is given in the [Appendix](#). We draw the conclusion that this is a widely applicable model capable of addressing different space and astrophysical situations.

3. Parametric Analysis and Discussion

As mentioned above, the trapped ion distribution function must be positive so that it represents a physically acceptable state. Imposing this requirement, we arrive at an inequality between the amplitude (ψ) and the width (δ) of the potential.

This width-amplitude relation (inequality) must be satisfied in order for the ion-hole excitations (BGK modes) predicted by the model to be physically meaningful. Figures 1–4 show the width-amplitude relations for different parameters. The area enclosed by the curves for a given range of ψ and δ represents potential parameters that can support a physically plausible BGK equilibrium. Figure 1 represents the case when the temperature ratio is 0.5 and Figure 2 represents the case when the temperature ratio is 3. It is interesting to note that for a vanishing value of the Havnes parameter that is in the limit $H = 0$, our theoretical results essentially recover the results of Aravindakshan et al. (2020, 2021). Figure 1 (bottom right panel) and Figure 3 depict the width-amplitude relation for ion holes generated in an electron-ion (i.e., nondusty) plasma ($H = 0$) for temperature ratios 0.5 and 3, respectively. In Figures 1–4, we have depicted the width-amplitude relation for different values of the temperature ratios and of the Havnes parameter. The inequality is satisfied (and thus ion holes may

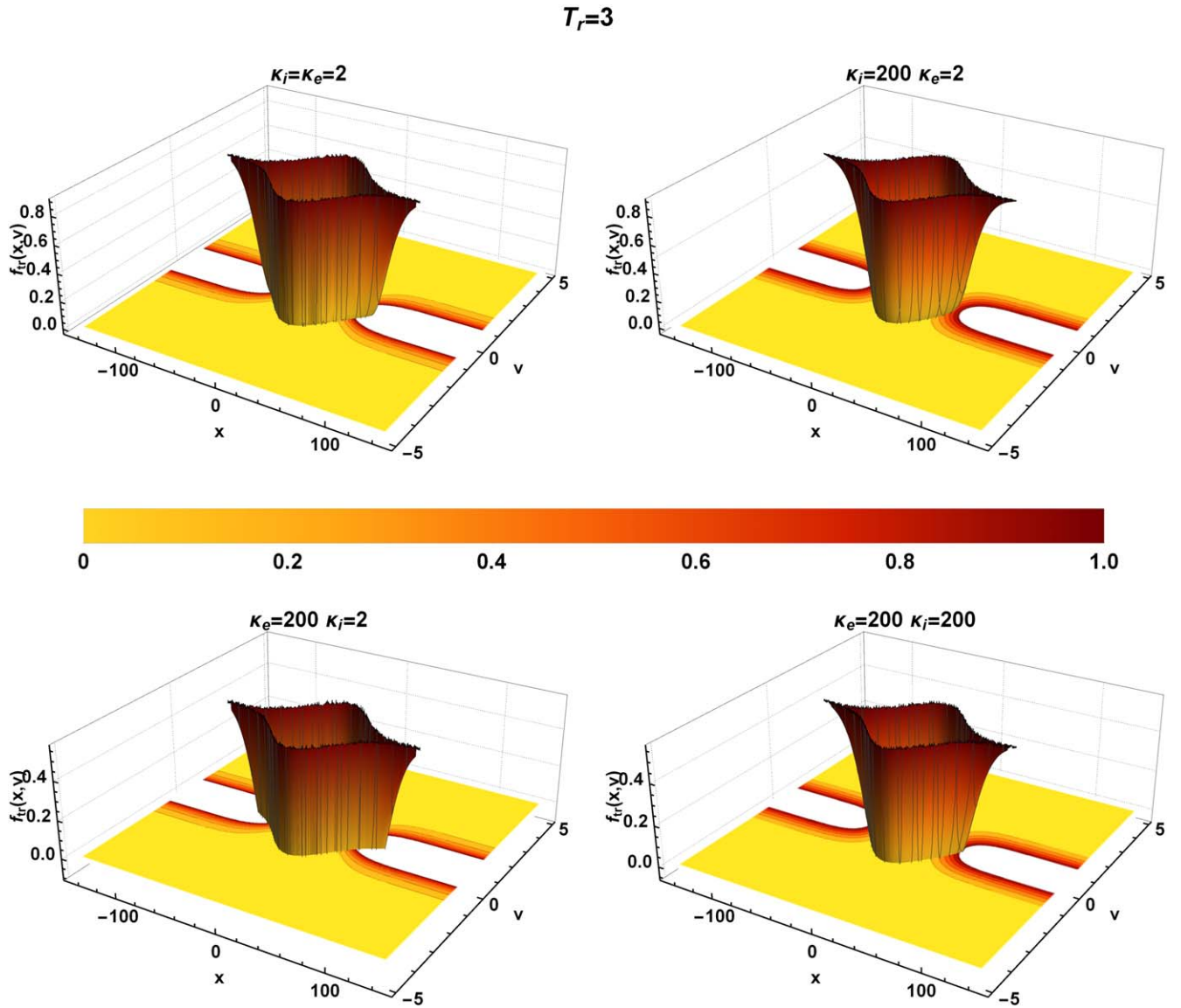


Figure 9. The structure of the trapped ion distribution function is depicted here. The Havnes parameter H is set to 0.1. Here $T_r = 3$, and different panels show the trapped ion distribution function for various kappa indices. At the bottom, the contour plot of the passing distribution function is also given.

exist) in the blue region or in the area marked by the curves in these region plots.

Figure 1 depicts the width-amplitude relation for an indicative ion-to-electron temperature ratio of $T_r = 0.5$. Different subpanels correspond to different values of the Havnes parameter. The kappa distribution is an efficient tool in modeling particle distribution deviating from thermal (Maxwell-Boltzmann) equilibrium, as observed in space; see, e.g., Livadiotis & McComas (2013) and Livadiotis (2015). It can be inferred from these diagrams—see Figure 1 (in comparison to the traditional picture represented in magenta, where both components practically follow a Maxwellian distribution)—that when the ions and/or the electrons follow the kappa distribution, the range of values of ψ and δ that can BGK modes is strongly modified. Recalling that low kappa values physically reflect the existence of highly energetic (accelerated) particles in the superthermal part of the distribution (while high kappa values, e.g., above 10, practically recover the Maxwellian behavior), we note that the occurrence of accelerated electrons results in a significant enlargement of the existence

region (see the green curve in Figure 1). Suprathermal electrons thus favor larger amplitude ion-holes—with similar impact expected in the associated bipolar electric field forms. The inverse effect is witnessed when suprathermal ions and quasi-Maxwellian electrons are considered (see the red curve in Figure 1) when the existence region for BGK modes actually shrinks slightly (predicting smaller amplitude ion-holes for a given width, e.g.), in comparison with the bottom right panel (where both species are assumed to be Maxwellian).

Interestingly, when a higher ion-to-electron temperature ratio is considered, a forbidden band (a gap) appears, dividing the existence region into two parts, as shown in Figures 3 and 4 (note, for reference, the bottom right panel in Figure 3 in the quasi-Maxwellian large kappa case, to begin with). When both species follow a quasi-Maxwellian distribution (large kappa), as depicted in the bottom right panel, large amplitude solutions are preferred. The same trend is followed when the ions are thermal and electrons are nonthermal (bottom left panel). However, when the ions are nonthermal, only small-amplitude solutions are preferred (see the top panels of the Figure 3).

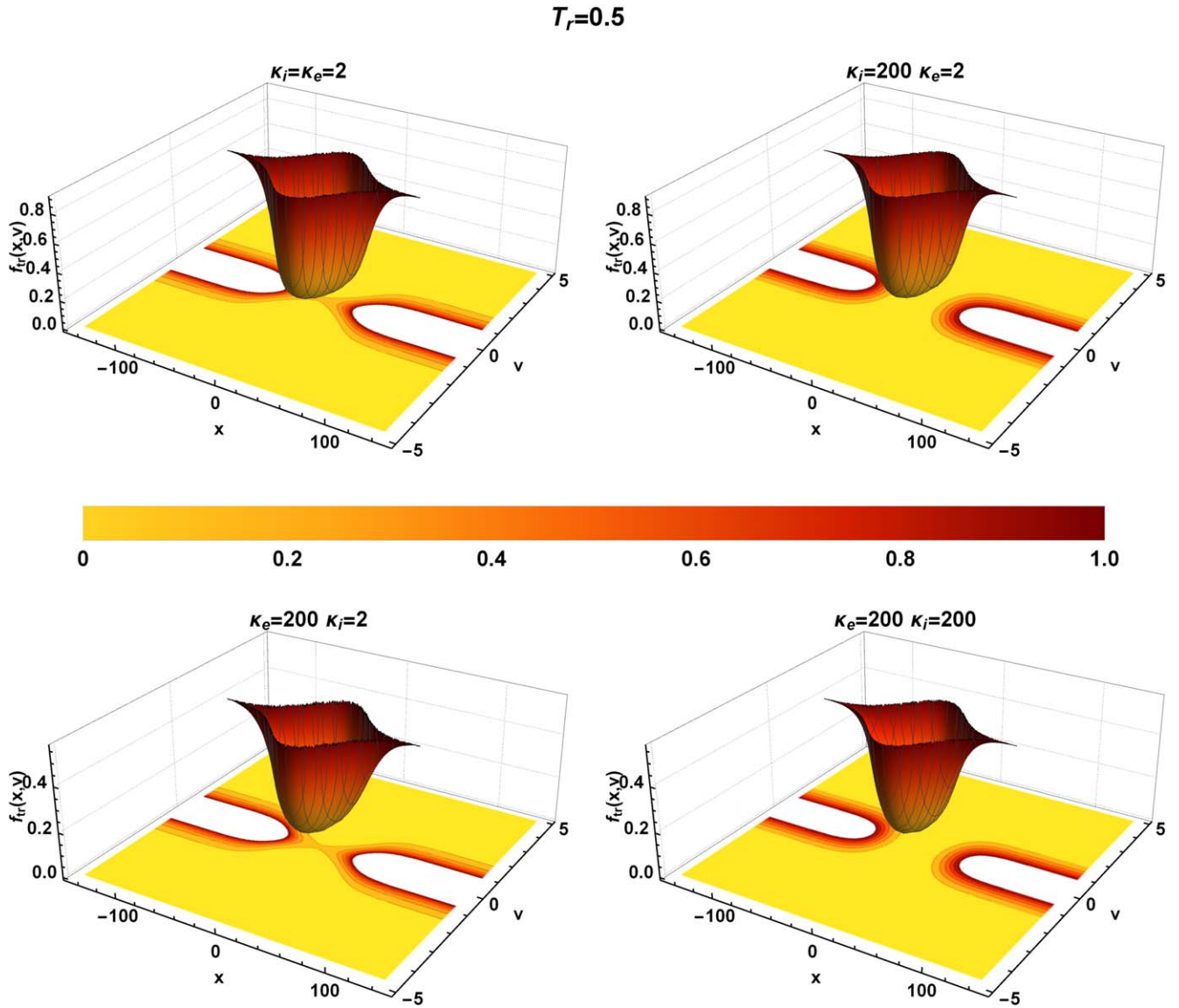


Figure 10. The structure of the trapped ion distribution function is depicted here. The Havnes parameter H is set to 0.5. Here $T_r = 0.5$, and different panels show the trapped ion distribution function for various kappa indices. At the bottom, the contour plot of the passing distribution function is also given.

In the case of Figure 4, it appears that small-amplitude or/and small-width solutions are excluded in this case, except for a thick region of ultra-small amplitude (but arbitrary width), which shrinks substantially for small electron kappa (dominant superthermal electron component)—see the top left and bottom left panels in Figure 4—but is slightly extended if the ions are kappa-distributed (with low kappa) instead—see the top right panel in the same figure.

It can be seen that when the dust density increases, the effect of the temperature ratio fades, while the forbidden region disappears, as is evident in Figures 1 and 2 (see the subpanels for $H = 0.3$ and 0.7). It is clear that for different values of the spectral index, there is a slight change in the permitted region, but the effect of the background plasma distribution is rather negligible.

The effect of the dust is further validated in Figures 5, 6 and 7, where we have tried to analyze the behavior of the trapped ion distribution function in terms of the total energy w . The differently colored lines in each panel illustrate the spectral index effect, while a comparison of the successive subpanels

shows that the curve completely overlaps with the curve derived from the actual formulas for the Maxwellian case. This indicates that our model, as formulated algebraically, adequately addresses BGK modes that formed in thermal (Maxwellian) plasmas as well, as expected. Figure 5 shows the case when the Havnes parameter is 0.1. As we can see, as we increase the temperature ratio, a small nondifferentiable part (i.e., with a discontinuity in the slope) appears in the curve in the region corresponding to the forbidden gap. This shows that the interaction between electrons and ions is intensified with an increase in the ion temperature. Physically speaking, when ions with a very high temperature become trapped inside the potential, they will oscillate with a very high amplitude. As a result, a small perturbation from the electrons might help the ions to overcome the trap and thus contribute to the free (passing) component. This also accounts for the presence of the forbidden gap in the width-amplitude relation, as shown in Figures 3 and 4. However, as expected, Figures 6 and 7 consist of smooth curves, indicating that the effect of dust in the physical plausibility of ion BGK modes. If we focus on the

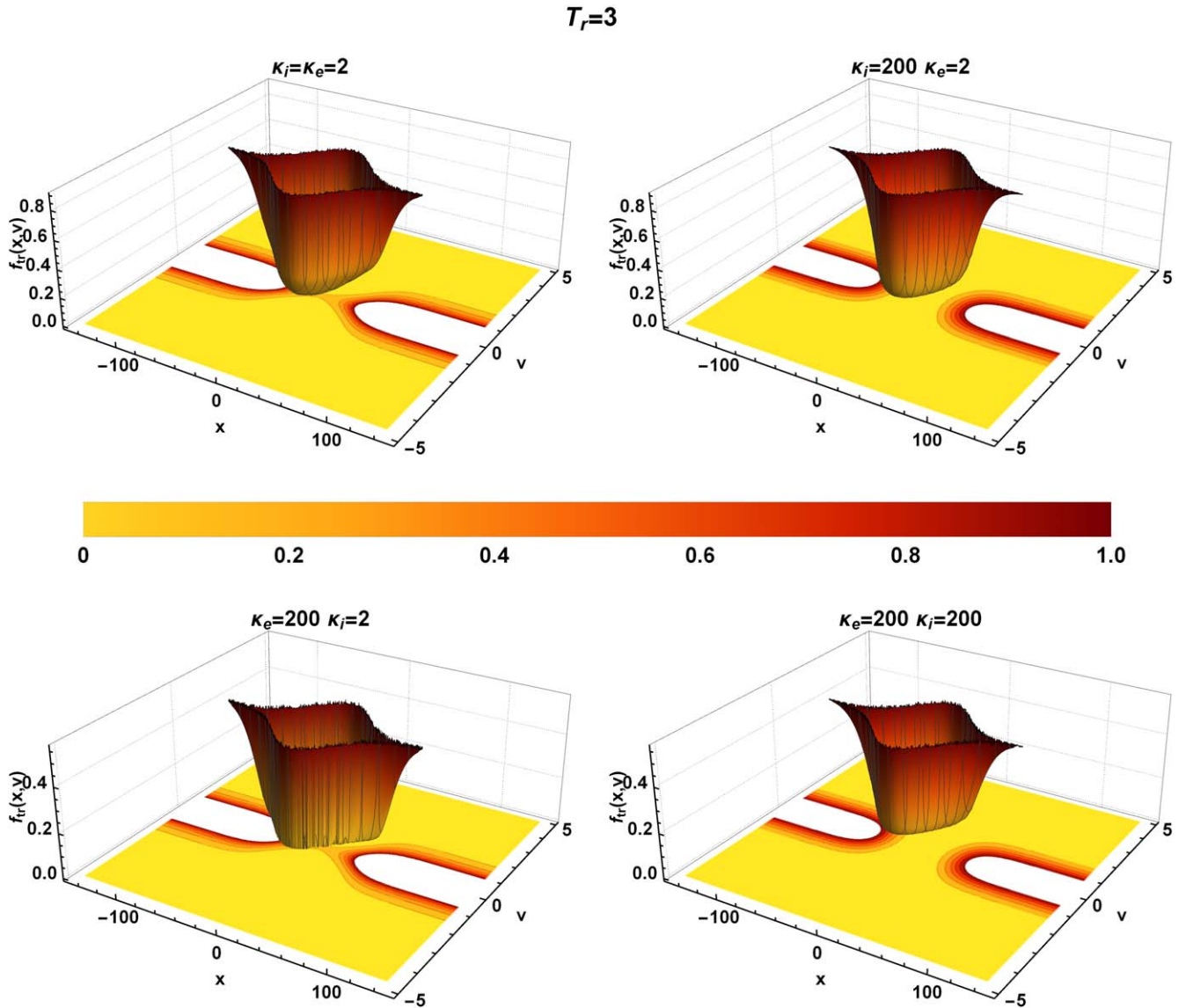


Figure 11. The structure of the trapped ion distribution function is depicted here. The Havnes parameter H is set to 0.5. Here $T_r = 3$, and different panels show the trapped ion distribution function for various kappa indices. At the bottom, the contour plot of passing distribution function is also given.

case where the electrons are thermally distributed (i.e., for very high values of κ_e) while the ions are kappa-distributed (i.e., for low κ_i), we can see that there is a tendency for the trapped distribution function to become negative. This indicates a physically unacceptable analytical solution, suggesting that BGK hole formation is not possible in this case. This is intuitively expected because electrons are easily energized and thus tend to deviate from thermal equilibrium, so that this scenario is not realistic. The role of the background plasma distribution function is well described here. At closer look, this effect is also evident in the case of significant dust density, as shown in Figure 7. This fact suggests that superthermal nature of the ions tends to prevent the generation of BGK modes, hence the presence of dust particles suppresses these predicted effects, thus favoring the generation of ion holes.

To gain insight into the qualitative impact of the relevant plasma configurational parameters, it may be appropriate to look at the behavior of the trapped ion distribution function as it appears in phase-space $\{x, v\}$. Figures 8 and 9 represent the

phase-space description of the trapped ion distribution function in a low dust density scenario. It can be seen from Figure 8 that when the plasma is entirely nonthermal, they form deeper and denser holes. As the spectral indices increase, they form shallow holes with a lower density for a lower temperature ratio. However, when the temperature ratio is higher, as given in Figure 9, there exists a strong interaction between the trapped ions and passing electrons, and as a result, the width and depth of the trapped distribution function is significantly affected around the center. Thus it can be inferred that due to the interaction of electrons with the trapped ions, a bunching of ions occurs at the center of the potential. It should be noted that as we move to higher dust density, as shown in Figures 10 and 11, even the higher temperature ratios cannot even modify the trapped distribution structure. In Figures 8–11, we have also given the contour plot of the passing particles. As expected, the passing ion density shows a dip at the center of the hole, and as we move away, the passing density increases.

4. Conclusions

In this paper, we have presented a theoretical model for ion BGK modes in a dusty plasma environment. As the model is developed assuming that the electrons and ions follow a superthermal distribution, this model can be used to predict and study the ion-hole structures that formed in the space/astrophysical plasmas. We have focused on various combinations of plasma systems in the current study, showing that this model can be applied to a wide variety of space/astrophysical environments. The observations of electrostatic solitary waves from the Saturn magnetosphere confirm that solitary wave structures are greatly affected by the dust present in the system (Pickett et al. 2015). Additionally, the presence of ion beams in the magnetospheres of Saturn and its moons suggests the possibility that ion BGK modes are generated (Holmberg et al. 2012, 2017). Thus, a BGK model that considers the effect of dust on the characteristics of ion BGK modes is imperative, and this study satiates this need. The theory revealed that the ion BGK modes are more physically plausible in a dusty plasma environment than in the typical plasma environment. The behavior of the width-amplitude relation and trapped distribution function for various dust densities revealed that the dust particles control the interaction of electrons with the formed potential.

Our analysis showed that dust-ion BGK modes are more physically plausible when the electron temperature is higher than the ion temperature. However, these effects become less significant when the dust density is higher. Interestingly, a forbidden band (a gap) appears in the width-amplitude plot when the temperature of the ions is higher than that of the electrons. Nevertheless, when we increase the dust density, this forbidden gap disappears. Moreover, the analysis of the trapped ion distribution function signals that the plasma system where electrons are in thermal equilibrium and the ions follow the kappa distribution is the least preferred system for generating ion BGK modes. It should be noted that all the values that we used in the numerical analysis are actually observed in the magnetospheres of Saturn and its moon, hence the results mentioned in the paper may provide the prediction of the characteristics of ion holes (BGK modes) generated in the Saturn magnetosphere.

In our model, we have assumed that the ion holes that formed in dusty plasmas are stationary. However, these structures move with finite velocities. Earlier, Bujarbarua & Schamel (1981), and more recently, computational studies (Jenab et al. 2021), have provided approximate ion-hole solutions moving at a certain speed u_0 . An extension of the theory presented here that takes into account a finite hole propagation speed forms the part of future planned work.

The authors gratefully acknowledge financial support from the Abu Dhabi Department of Education and Knowledge (ADEK), currently ASPIRE UAE, via an Abu Dhabi Award for Research Excellence (AARE-2018)—research grant ADEK/HE/157/18. I.K. acknowledges financial support from Khalifa University of Science and Technology, Abu Dhabi UAE via the (internal funding) project FSU-2021-012/8474000352, in addition to Khalifa University Space and Planetary Science Center under grant No. KU-SPSC-8474000336. This work was carried out during a visit by Harikrishnan Aravindakshan to Khalifa University; the hospitality offered by the host is gratefully acknowledged.

Data Availability: No new data were generated or analyzed in support of this research.

Appendix Bernstein–Greene–Kruskal Ion Modes in Thermal Dusty Plasma

Let us assume that both electrons and ions follow the Maxwell-Boltzmann distribution function. Taking the first moment of the distribution function, we obtain the electron density given by

$$n_e = \exp(T_r \phi). \quad (\text{A1})$$

Here, we have defined the temperature ratio $T_r = T_i/T_e$. As mentioned above, the ions follow a thermal distribution,

$$f_i(v) = \frac{1}{\sqrt{\pi}} \exp(-v^2). \quad (\text{A2})$$

Following the BGK scheme, we assume a frame in which both the potential pulse and the ion distribution are in a self-consistent steady state. Working in this frame, we write the ion distribution function in terms of the normalized total energy of the particles as

$$w = \frac{1}{2}(v^2 + \phi). \quad (\text{A3})$$

Now we change the variable $[(x, v) \rightarrow w]$, that is, we move to the energy frame w . Thus, the normalized distribution function transforms as

$$f_i(w) = \frac{1}{\sqrt{\pi}} \exp(-w), \quad (\text{A4})$$

where

$$f(x, v)dv = f(w)dw/\sqrt{2w - \phi}.$$

As mentioned above, let us assume the electrostatic potential in the Gaussian form given by

$$\phi(x) = -\psi \exp\left(-\frac{x^2}{2\delta^2}\right), \quad (\text{A5})$$

where ψ is the amplitude, and δ is the width of the perturbation, respectively. δ is a distance at which the potential decreases to 0.6065 times the maximum amplitude of ψ . The FWHM of the perturbation is given by $\Delta = 2.35 \delta$. Similarly as mentioned above, the passing particle distribution function is denoted by f_p , and the trapped particle is denoted by f_{tr} . Equation (2) can be written as

$$\frac{d^2\phi}{dx^2} = (1 - H)n_e - n_{i,p} - n_{i,tr} + H. \quad (\text{A6})$$

The passing ion density is given by

$$n_{i,p} = \int_{-\infty}^{-\sqrt{-\phi}} f_p(x, v)dv + \int_{+\sqrt{-\phi}}^{\infty} f_p(x, v)dv \quad (\text{A7})$$

Exploiting the symmetry of the Maxwell-Boltzmann distribution (i.e., a pair function of the velocity argument), we can

write n_p as

$$n_{i,p} = 2 \int_{+\sqrt{-\phi}}^{\infty} f_p dv = 2 \left(\int_0^{\infty} f_p dv - \int_0^{\sqrt{-\phi}} f_p dv \right). \quad (\text{A8})$$

Now Equation (A8) can be expanded as

$$n_{i,p} = 1 - \text{erf}(\sqrt{-\phi}), \quad (\text{A9})$$

where $\text{erf}(x)$ denotes the error function. Now that we have obtained the passing ion density, we can derive the trapped ion density by rearranging Equation (A6). We obtain the trapped electron density as

$$n_{i,\text{tr}} = (1 - H) \exp(T_r \phi) + \frac{2\phi \log\left(-\frac{\phi}{\psi}\right)}{\delta^2} + \frac{\phi}{\delta^2} - 1 - \text{erf}(\sqrt{-\phi}) + H. \quad (\text{A10})$$


For convenience, we make a transformation $-\phi \rightarrow \rho$ and obtain the trapped ion density as

$$n_{i,\text{tr}} = (1 - H) \exp(-T_r \rho) + 1 - \frac{2\rho \log\left(\frac{\rho}{\psi}\right)}{\delta^2} - \frac{\rho}{\delta^2} - 1 + \text{erf}[\sqrt{\rho}] + H. \quad (\text{A11})$$

Following the same method as in the above section, we obtain the trapped ion distribution function for Maxwellian plasmas,

$$f_{tr,i}(w) = -(1 - H) \frac{T_r \sqrt{-w} e^{2T_r w} \text{erf}(\sqrt{2} \sqrt{T_r w})}{\sqrt{\pi} \sqrt{T_r w}} + \frac{\exp(w) I_0(w)}{\sqrt{\pi}} - \frac{4\sqrt{2} \sqrt{-w} \left(\log\left(-\frac{8w}{\psi}\right) - 2 \right)}{\pi \delta^2} - \frac{6\sqrt{2} \sqrt{-w}}{\pi \delta^2} \quad (\text{A12})$$

ORCID iDs

Harikrishnan Aravindakshan  <https://orcid.org/0000-0003-4663-4255>

Amar Kakad  <https://orcid.org/0000-0002-1308-4245>

Bharati Kakad  <https://orcid.org/0000-0001-8440-3373>
Ioannis Kourakis  <https://orcid.org/0000-0002-4027-0166>

References

- Aravindakshan, H., Kakad, A., & Kakad, B. 2018a, *PhPI*, **25**, 052901
Aravindakshan, H., Kakad, A., & Kakad, B. 2018b, *PhPI*, **25**, 122901
Aravindakshan, H., Kakad, A., Kakad, B., & Yoon, P. H. 2021, *Plasma*, **4**, 435
Aravindakshan, H., Yoon, P. H., Kakad, A., & Kakad, B. 2020, *MNRAS*, **497**, L69
Badman, S. V., Achilleos, N., Arridge, C. S., et al. 2012a, *JGRA*, **117**, A01211
Badman, S. V., Achilleos, N., Arridge, C. S., et al. 2012b, *JGRA*, **117**, A04220
Bernstein, I. B., Greene, J. M., & Kruskal, M. D. 1957, *PhRv*, **108**, 546
Bujarbarua, S., & Schamel, H. 1981, *JPIPh*, **25**, 515
Eliasson, B., & Shukla, P. 2006a, *PhR*, **422**, 225
Eliasson, B., & Shukla, P. K. 2006b, *PhR*, **422**, 225
Farrell, W., Wahlund, J.-E., Morooka, M., et al. 2017, *JGRE*, **122**, 729
Franck, C., Klinger, T., Piel, A., & Schamel, H. 2001, *PhPI*, **8**, 4271
Franz, J. R., Kintner, P. M., & Pickett, J. S. 1998, *GeoRL*, **25**, 1277
Hapgood, M., Perry, C., Davies, J., & Denton, M. 2011, *P&SS*, **59**, 618
Hellberg, M., Mace, R., Baluku, T., Kourakis, I., & Saini, N. 2009, *PhPI*, **16**, 094701
Holmberg, M. K., Wahlund, J.-E., Morooka, M., & Persoon, A. 2012, *P&SS*, **73**, 151
Holmberg, M. K. G., Shebanits, O., Wahlund, J.-E., et al. 2017, *JGRA*, **122**, 12,258
Jenab, S. M. H., Brodin, G., Juno, J., & Kourakis, I. 2021, *NatSR*, **11**, 16358
Kakad, A., Kakad, B., Anekallu, C., et al. 2016, *JGRA*, **121**, 4452
Kakad, B., Kakad, A., Aravindakshan, H., & Kourakis, I. 2022, *ApJ*, **934**, 126
Krasovsky, V. L., Matsumoto, H., & Omura, Y. 2003, *JGRA*, **108**, 1117
Livadiotis, G. 2015, *JGRA*, **120**, 1607
Livadiotis, G., & McComas, D. 2013, *SSRv*, **175**, 183
Luque, A., & Schamel, H. 2005, *PhR*, **415**, 261
Matsumoto, H., Kojima, H., Miyatake, T., et al. 1994, *GeoRL*, **21**, 2915
McFadden, J., Carlson, C., Ergun, R., et al. 2003, *JGRA*, **108**, 8018
Omura, Y., Matsumoto, H., Miyake, T., & Kojima, H. 1996, *JGRA*, **101**, 2685
Pécseli, H., Trulsen, J., & Armstrong, R. 1984, *PhyS*, **29**, 241
Pickett, J., Kurth, W., Gurnett, D., et al. 2015, *JGRA*, **120**, 6569
Pécseli, H., Armstrong, R., & Trulsen, J. 1981, *PhLA*, **81**, 386
Pécseli, H. L. 1987, *LPB*, **5**, 211
Schamel, H. 1986, *PhR*, **140**, 161
Shukla, P. K., & Mamun, A. 2015, *Introduction to Dusty Plasma Physics* (Boca Raton, FL: CRC Press)
Singh, K., Kakad, A., Kakad, B., & Ioannis, K. 2022, *A&A*, in press
Singh, K., Kakad, A., Kakad, B., & Saini, N. S. 2021, *MNRAS*, **500**, 1612
Wang, R., Vasko, I., Mozer, F., et al. 2020, *ApJL*, **889**, L9
Williams, J., Chen, L.-J., Kurth, W., Gurnett, D., & Dougherty, M. 2006, *GeoRL*, **33**, L06103
Yaroshenko, V., & Lühr, H. 2016, *Icar*, **278**, 79
Yaroshenko, V., Verheest, F., & Morfill, G. 2007, *A&A*, **461**, 385